CHEMISTRY OF MATERIALS
Article

Chem. Mater. **2010,** *22,* 2635–2645 2635
DOI:10.1021/cm1000208

Observation and Isolation of Layered and Framework Ytterbium Hydroxide Phases Using In Situ Energy-Dispersive X-ray Diffraction

Laura J. McIntyre,[†] Timothy J. Prior,[‡] and Andrew M. Fogg*[,†]

[†]*Department of Chemistry, University of Liverpool, Liverpool, L69 7ZD, United Kingdom, and*
[‡]*Department of Chemistry, University of Hull, Kingston upon Hull, HU6 7RX, United Kingdom*

Received January 4, 2010. Revised Manuscript Received February 22, 2010

In situ energy-dispersive X-ray diffraction has been used to investigate the synthesis of the recently reported lanthanide hydroxynitrate phases, $Ln_2(OH)_5NO_3 \cdot 1.5H_2O$ (Ln = Y, Er, Yb). Through control of the reaction temperature, three distinct layered phases with differing degrees of hydration ($x = 1$ (**1**), 1.5 (**2**), and 2 (**3**)) were observed in the Yb synthesis and subsequently isolated. Only the phase with $x = 1.5$ was observed for the reactions with Y and Er. The crystal structures of $Yb_2(OH)_5NO_3 \cdot 2H_2O$ (**2**) and $Yb_2(OH)_5NO_3 \cdot H_2O$ (**3**) were determined in a single-crystal diffraction study and represent the first crystal structures of the new lanthanide hydroxynitrate phases. Both $Yb_2(OH)_5NO_3 \cdot 2H_2O$ and $Yb_2(OH)_5NO_3 \cdot H_2O$ adopt orthorhombic structures in which the nitrate anion is coordinated to the Yb^{3+} cations within the hydroxide layer and are largely resistant to anion exchange. This is in contrast to the $Ln_2(OH)_5NO_3 \cdot 1.5H_2O$ phases, which undergo facile anion exchange reactions at room temperature, indicating that the nitrate resides in the interlayer gallery. At temperatures above 200 °C, the three layered phases were determined to be intermediates in the synthesis of $Yb_4O(OH)_9NO_3$ (**4**), which has a framework structure with the uncoordinated nitrate anions located in one-dimensional channels. The in situ diffraction technique has allowed for a detailed kinetic and mechanistic investigation of the synthesis and revealed that the layered ytterbium hydroxynitrate phases form via a two-dimensional phase boundary-controlled growth mechanism. It was also possible to estimate the activation energies for the hydrothermal synthesis of $Yb_2(OH)_5NO_3 \cdot H_2O$ and $Yb_2(OH)_5NO_3 \cdot 2H_2O$ from basic solution, as +29 and +67 kJ/mol, respectively.

Introduction

Intercalation chemistry provides a method of controlling and modifying the properties of a host lattice while having only a minimal effect on the structure; as a result, it has been the focus of numerous investigations over many years, leading to applications in a diverse range of fields. One family of materials that has received considerable attention, because of their compositional flexibility and varied range of applications, is the layered double hydroxides (LDHs).[1−3] These anion-exchange host lattices typically combine a divalent cation (e.g., Mg^{2+}, Zn^{2+}, Co^{2+}, Ni^{2+}) and a trivalent cation (e.g., Al^{3+}, Cr^{3+}, Fe^{3+}, Ga^{3+}) in the hydroxide layers, with a charge-balancing inorganic or organic anion in the interlayer gallery.

Despite the compositional flexibility of the LDHs, the incorporation of lanthanide cations into these materials has been limited to immobilizing Eu^{3+} and Gd^{3+} in the interlayer space.[4] The inclusion of lanthanide cations into the hydroxide layers offers the potential to combine the optical, magnetic, and catalytic properties of the lanthanides with the flexibility of intercalation hosts. The hydrothermal synthesis of a new family of anion-exchange materials containing either the smaller lanthanide cations or yttrium, with the composition $Ln_2(OH)_5NO_3 \cdot 1.5H_2O$ (Ln = Y, Gd−Lu), was recently reported.[5,6] In this study, the flexibility of the materials toward anion exchange was demonstrated by their facile reactions with carboxylate and sulfonate anions at room temperature. Moreover, it was noted that the materials containing the smallest lanthanides (Yb and Lu) were always biphasic. Previous studies had been limited to the synthesis of $Yb_2(OH)_5NO_3 \cdot 2H_2O$ and $Y_2(OH)_5NO_3 \cdot 2H_2O$,[7−9] and the larger lanthanides are known to form layered hydroxides with the composition $Ln(OH)_2NO_3 \cdot xH_2O$ (Ln = La, Pr−Nd, Sm, and Gd).[10−13] In the latter materials, the

*Author to whom all correspondence should be addressed. Tel.: +44 151 794 2047. Fax: +44 151 794 3587. E-mail: afogg@liverpool.ac.uk.

(1) Evans, D. G.; Slade, R. C. T. *Struct. Bonding* (*Berlin*) **2006**, *119*, 1.
(2) Feng, L.; Duan, X. *Struct. Bonding* (*Berlin*) **2006**, *119*, 193.
(3) Sels, B. F.; De Vos, D. E.; Jacobs, P. A. *Catal. Rev. Sci. Eng.* **2001**, *43*, 443.
(4) Gago, S.; Pillinger, M.; Ferreira, R. A. S.; Carlos, L. D.; Santos, T. M.; Goncalves, I. S. *Chem. Mater.* **2005**, *17*, 5803.
(5) McIntyre, L. J.; Jackson, L. K.; Fogg, A. M. *J. Phys. Chem. Solids* **2008**, *69*, 1070.
(6) McIntyre, L. J.; Jackson, L. K.; Fogg, A. M. *Chem. Mater.* **2008**, *20*, 335.
(7) Haschke, J. M. *Inorg. Chem.* **1974**, *13*, 1812.
(8) Holcombe, C. E. *J. Am. Ceram. Soc.* **1978**, *61*, 481.
(9) Schildermans, I.; Mullens, J.; Yperman, J.; Franco, D.; Vanpoucke, L. C. *Thermochim. Acta* **1994**, *231*, 185.
(10) Louer, D.; Louer, M. *J. Solid State Chem.* **1987**, *68*, 292.
(11) Louer, M.; Louer, D.; Delgado, A. L.; Martinez, O. G. *Eur. J. Solid State Inorg. Chem.* **1989**, *26*, 241.
(12) Lundberg, M.; Skarnulis, A. J. *Acta Crystallogr., Sect. B: Struct. Crystallogr. Cryst. Chem.* **1976**, *32*, 2944.

Published on Web 03/04/2010

nitrate anion is directly bound to the lanthanide cation, but anion exchange was shown for the reaction of $La(OH)_2NO_3 \cdot xH_2O$ with carboxylate anions, following prolonged heating at 60 °C.[14]

Subsequent studies have extended the range of compounds in the $Ln_2(OH)_5X \cdot xH_2O$ family of anion exchange host lattices. Variation of the synthetic conditions has allowed some of the larger lanthanides, including Eu and Sm, to be incorporated into the hydroxide layers.[15−17] In addition, the related halide phases, $Ln_2(OH)_5X \cdot 1.5H_2O$ (Ln = Y, Nd−Lu; X = Cl, Br) have been prepared. These materials were the first of this family to be structurally characterized. Two polymorphs—orthorhombic and monoclinic—of $Yb_2(OH)_5Cl \cdot 1.5H_2O$ have been identified, and both contain eight and nine coordinate lanthanides with bridging μ_3-hydroxide anions.[18] The water molecules are bound to the lanthanide cations within the layers and Cl^- anions occupy the interlayer gallery. The polymorphism results from subtle differences in the orientation of the polyhedra and the presence of disordered water molecules in the orthorhombic structure.[18] The orthorhombic structures of $Ln_2(OH)_5Cl \cdot 1.5H_2O$ (Ln = Nd−Er, Y) have been independently determined from powder XRD data.[19] The layer structure in these phases is similar to that reported for $[Yb_4(OH)_{10}(H_2O)_4]$AQDS and $[Y_4(OH)_{10}(H_2O)_4]$NDS (where AQDS represents anthraquinonedisulfonate and NDS represents 2,6-naphthalenedisulfonate), but the lower hydration level in the chloride materials results in fewer nine-coordinated lanthanide polyhedra, which alters the topology of the layers.[20]

Potential applications of these materials, other than as anion exchangers, have also been demonstrated. Photoluminescence has been observed from $Tb_2(OH)_5Cl \cdot 1.5H_2O$[19] and $Eu_2(OH)_5Cl \cdot 1.5H_2O$.[15] In addition, Eu-doped films of $Gd_2(OH)_5Cl \cdot 1.5H_2O$ have been prepared, with greatly enhanced photoluminescence being observed from the calcined films, compared to hydroxide ones.[21] The Gd hydroxychloride has been proposed as a potential MRI contrast agent,[22] and $[Yb_4(OH)_{10}(H_2O)_4]$AQDS has been shown to be an effective catalyst for the oxidation of organic sulfides.[20]

The majority of these new lanthanide hydroxy salts are synthesized hydrothermally and the nature of this technique means that there is generally little knowledge of the reaction kinetics and pathways that are taken. Time-resolved, in situ, energy-dispersive X-ray diffraction (EDXRD) has been proven to be a powerful tool in the study of such reactions revealing detailed kinetic and mechanistic information on a wide range of solid-state reactions by allowing the reactions to be continuously monitored.[23−25] The technique has been used to investigate systems as diverse as mesoporous silicates[26] and metallocene intercalates of layered chalcogenides.[27] Notable discoveries include staging in the anion-exchange reactions of LDHs,[28−30] kinetic and thermodynamic control in highly selective anion-exchange reactions,[31,32] and lower dimensional intermediates in the formation of microporous phosphates.[33−35]

In a previous paper, it was noted that, of the $Ln_2(OH)_5NO_3 \cdot 1.5H_2O$ compounds, those containing Yb and Lu displayed a second phase with a slightly larger interlayer separation of ~9.4 Å.[6] Here, we report the findings of a time-resolved in situ EDXRD study of the formation of $Yb_2(OH)_5NO_3 \cdot 1.5H_2O$, which revealed three different layered phases and the ultimate transformation to a three-dimensional (3D) framework structure, $Yb_4O(OH)_9NO_3$. Structures for three of the phases are reported, and a kinetic analysis of the system is presented.

Experimental Section

Synthesis. The $Ln_2(OH)_5NO_3 \cdot xH_2O$ (Ln = Y, Er, Yb) phases were synthesized via a hydrothermal route, as described previously.[6] In a typical reaction, 7.5 mL of a 0.44 M $Ln(NO_3)_3 \cdot xH_2O$ aqueous solution is added to 2.5 mL of an aqueous solution containing 2.10 M NaOH and 1.44 M $NaNO_3$ in a Teflon-lined autoclave. The resulting mixture was treated hydrothermally at a temperature of 100−220 °C. $Yb_4O(OH)_9NO_3$ was synthesized from the same reagent mixture at temperatures above 200 °C on the time scales investigated here. In all cases, the resulting solid was filtered, washed, and allowed to dry in air. Anion-exchange reactions were performed by suspending 75 mg of $Yb_2(OH)_5NO_3 \cdot 2H_2O$ (**2**), $Yb_2(OH)_5NO_3 \cdot H_2O$ (**3**), or $Yb_4O(OH)_9NO_3$ (**4**) in 5 mL of an aqueous solution containing a 3-fold molar excess of disodium terephthalate at

(13) Mullica, D. F.; Sappenfield, E. L.; Grossie, D. A. *J. Solid State Chem.* **1986**, *63*, 231.
(14) Newman, S. P.; Jones, W. *J. Solid State Chem.* **1999**, *148*, 26.
(15) Geng, F. X.; Xin, H.; Matsushita, Y.; Ma, R. Z.; Tanaka, M.; Izumi, F.; Iyi, N.; Sasaki, T. *Chem.—Eur. J.* **2008**, *14*, 9255.
(16) Hindocha, S. A.; McIntyre, L. J.; Fogg, A. M. *J. Solid State Chem.* **2009**, *182*, 1070.
(17) Lee, K. H.; Byeon, S. H. *Eur. J. Inorg. Chem.* **2009**, 929.
(18) Poudret, L.; Prior, T. J.; McIntyre, L. J.; Fogg, A. M. *Chem. Mater.* **2008**, *20*, 7447.
(19) Geng, F. X.; Matsushita, Y.; Ma, R. Z.; Xin, H.; Tanaka, M.; Izumi, F.; Iyi, N.; Sasaki, T. *J. Am. Chem. Soc.* **2008**, *130*, 16344.
(20) Gandara, F.; Perles, J.; Snejko, N.; Iglesias, M.; Gomez-Lor, B.; Gutierrez-Puebla, E.; Monge, M. A. *Angew. Chem., Int. Ed.* **2006**, *45*, 7998.
(21) Hu, L. F.; Ma, R. Z.; Ozawa, T. C.; Sasaki, T. *Angew. Chem., Int. Ed.* **2009**, *48*, 3846.
(22) Lee, B. I.; Lee, K. S.; Lee, J. H.; Lee, I. S.; Byeon, S. H. *Dalton Trans.* **2009**, 2490.
(23) O'Hare, D.; Evans, J. S. O.; Fogg, A.; O'Brien, S. *Polyhedron* **2000**, *19*, 297.
(24) Walton, R. I.; O'Hare, D. *Chem. Commun.* **2000**, 2283.
(25) Francis, R. J.; O'Hare, D. *J. Chem. Soc., Dalton Trans.* **1998**, 3133.
(26) O'Brien, S.; Francis, R. J.; Fogg, A.; O'Hare, D.; Okazaki, N.; Kuroda, K. *Chem. Mater.* **1999**, *11*, 1822.
(27) Evans, J. S. O.; Price, S. J.; Wong, H. V.; O'Hare, D. *J. Am. Chem. Soc.* **1998**, *120*, 10837.
(28) Fogg, A. M.; Dunn, J. S.; O'Hare, D. *Chem. Mater.* **1998**, *10*, 356.
(29) Williams, G. R.; Norquist, A. J.; O'Hare, D. *Chem. Mater.* **2004**, *16*, 975.
(30) Williams, G. R.; Fogg, A. M.; Sloan, J.; Taviot-Gueho, C.; O'Hare, D. *Dalton Trans.* **2007**, 3499.
(31) Fogg, A. M.; Dunn, J. S.; Shyu, S. G.; Cary, D. R.; O'Hare, D. *Chem. Mater.* **1998**, *10*, 351.
(32) Williams, G. R.; Dunbar, T. G.; Beer, A. J.; Fogg, A. M.; O'Hare, D. *J. Mater. Chem.* **2006**, *16*, 1231.
(33) Francis, R. J.; O'Brien, S.; Fogg, A. M.; Halasyamani, P. S.; O'Hare, D.; Loiseau, T.; Ferey, G. *J. Am. Chem. Soc.* **1999**, *121*, 1002.
(34) Loiseau, T.; Beitone, L.; Millange, F.; Taulelle, F.; O'Hare, D.; Ferey, G. *J. Phys. Chem. B* **2004**, *108*, 20020.
(35) Millange, F.; Walton, R. I.; Guillou, N.; Loiseau, T.; O'Hare, D.; Ferey, G. *Chem. Mater.* **2002**, *14*, 4448.

either room temperature or 60 °C for up to 7 days. The resulting solids were recovered by filtration and dried in air.

Characterization. Powder XRD patterns were recorded with Cu $K\alpha_1$ radiation on a Stoe Model Stadi-P diffractometer in either Bragg−Brentano or Debye−Scherrer geometry. A combination of thermogravimetric analysis (TGA) and elemental analysis was used to determine the stoichiometry of the materials. TGA traces were recorded on a Perkin−Elmer Model STA600 Simultaneous Thermal Analyzer. Inductively coupled plasma (ICP) analysis, to determine the metal content of the samples, was performed on a Ciros CCD optical emission spectrometer, following complete dissolution of the samples in dilute HNO_3 and CHN analysis was performed on a FlashEA 1112 instrument. Fourier transform infrared (FTIR) spectra were recorded on a Nicolet Model Nexus FT-IR spectrophotometer.

Structure Determination. Single-crystal XRD data were collected on the microcrystal diffraction facility of Station 9.8 at the UK Synchrotron Radiation Source STFC, Daresbury Laboratory. Crystals were covered in a thin film of perfluoropolyether oil and mounted at the end of a two-stage glass fiber and cooled in an Oxford Instruments nitrogen-gas cryostream to 120 K. Data were collected using a Bruker D8 diffractometer operating with an APEXII CCD area detector. Data collection nominally covered a sphere of reciprocal space in three series of ω-rotation exposure frames with different crystal orientation φ angles. Reflection intensities were integrated using standard procedures, allowing for the plane-polarized nature of the primary synchrotron beam. Semiempirical corrections were applied to account for absorption and incident beam decay. Unit-cell parameters were refined using all observed reflections in the complete datasets.

Structures were solved by routine automatic direct methods. The structures were completed by least-squares refinement based on all unique measured F^2 values and difference Fourier methods.

In Situ Diffraction. Time-resolved, in situ EDXRD experiments were performed on Station 16.4 of the U.K. Synchrotron Radiation Source, Daresbury Laboratory. The syntheses were performed on the same scale as that described above in Teflon-lined hydrothermal autoclaves that were heated in a temperature-controlled block. The autoclaves were modified by having their walls thinned to let the beam pass through and it is necessary to stir the reactions to maintain a suspension of the solid material in the beam. In these reactions, lanthanide $K\alpha$ resonances were observed alongside the Bragg reflections in the spectra and have a constant intensity throughout the reactions, indicating that a constant amount of sample is maintained in the beam. Full details of the station and the experimental setup can be found elsewhere.[29,36−38] In a typical experiment, the EDXRD spectra were collected with an acquisition time of 30 s at a fixed detector angle of either 1.75° or 1.83° 2θ. The reflection positions, measured in units of keV, can be converted to d-spacings, using the energy-dispersive form of Bragg's Law, $E = hc/(2d \sin\theta) = 6.19926/(d \sin\theta)$.

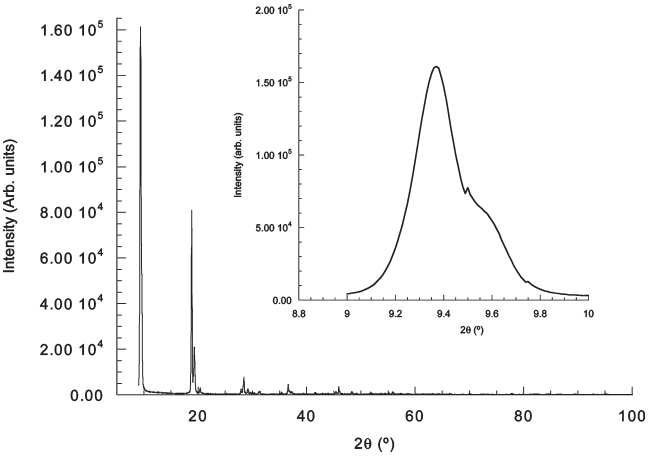

Figure 1. Powder XRD pattern of $Yb_2(OH)_5NO_3 \cdot 1.5H_2O$. (Inset shows an expanded view of the (002) reflection, indicating the presence of two phases).

Data analysis. Kinetic data were extracted for each reaction by integration of each Bragg reflection in each spectrum, using a Gaussian peak fitting routine.[39] The integrated areas were then converted to the extent of reaction at time t ($\alpha(t)$), using the relation $\alpha(t) = I_{hkl}(t)/I_{hkl}(\max)$, where $I_{hkl}(t)$ is the area of a given reflection at time t, and $I_{hkl}(\max)$ is the maximum area of that reflection. The $\alpha(t)$ data was then fitted with the Avrami−Erofe'ev rate expression.[40−44]

Results and Discussion

Materials Characterization. The hydrothermal synthesis of a new family of anion-exchangeable layered hydroxides incorporating the smaller lanthanides within the layers, $Ln_2(OH)_5X \cdot 1.5H_2O$ (Ln = Y, Gd−Lu; X = NO_3, Cl) recently has been reported.[5,6,18] In these studies, it was observed that, of these materials, those containing the smallest lanthanides, Yb and Lu, were not synthesized phase-pure; in both cases, a second phase displaying a slightly larger interlayer separation is apparent in the powder XRD data, as shown in Figure 1. In the case of the hydroxynitrate materials, this additional phase has an interlayer separation of ~9.4 Å, compared to the 9.2 Å spacing observed for the larger lanthanides and yttrium. The analysis of the Yb and Lu hydroxynitrate phases by TGA and elemental analysis is consistent with formula $Ln_2(OH)_5NO_3 \cdot 1.5H_2O$, suggesting that the 9.4 Å and 9.2 Å phases have a similar composition. The characterizing data for these phases are included in the Supporting Information.

The standard laboratory synthesis of the lanthanide hydroxynitrate materials, at 150 °C, was monitored by EDXRD, and the 3D stack plot of the spectra is shown in Figure 2a. From these data, the formation of the two distinct phases, with d-spacings of 9.2 and 9.4 Å, is apparent. It is also notable that the crystallization of these phases is a fast process occurring over the course of

(36) Clark, S. M.; Cernik, R. J.; Grant, A.; York, S.; Atkinson, P. A.; Gallagher, A.; Stokes, D. G.; Gregory, S. R.; Harris, N.; Smith, W.; Hancock, M.; Miller, M. C.; Ackroyd, K.; Farrow, R.; Frances, R.; O'Hare, D. *Eur. Powder Diffr.: EPDIC IV, Proc. Eur. Powder Diffr. Conf., 4th, 1995, Part 1−2* **1996**, *228*, 213.
(37) Clark, S. M.; Nield, A.; Rathbone, T.; Flaherty, J.; Tang, C. C.; Evans, J. S. O.; Francis, R. J.; O'Hare, D. *Nucl. Inst. Methods B* **1995**, *97*, 98.
(38) Evans, J. S. O.; Francis, R. J.; O'Hare, D.; Price, S. J.; Clark, S. M.; Flaherty, J.; Gordon, J.; Nield, A.; Tang, C. C. *Rev. Sci. Instrum.* **1995**, *66*, 2442.
(39) Clark, S. M. *J. Appl. Crystallogr.* **1995**, *28*, 646.
(40) Avrami, M. *J. Chem. Phys.* **1939**, *7*, 1103.
(41) Avrami, M. *J. Chem. Phys.* **1940**, *8*, 212.
(42) Avrami, M. *J. Chem. Phys.* **1941**, *9*, 177.
(43) Erofe'ev, B. V. *C. R. (Dokl.) Acad. Sci. URSS* **1946**, *52*, 511.
(44) Hancock, J. D.; Sharp, J. H. *J. Am. Ceram. Soc.* **1972**, *55*, 74.

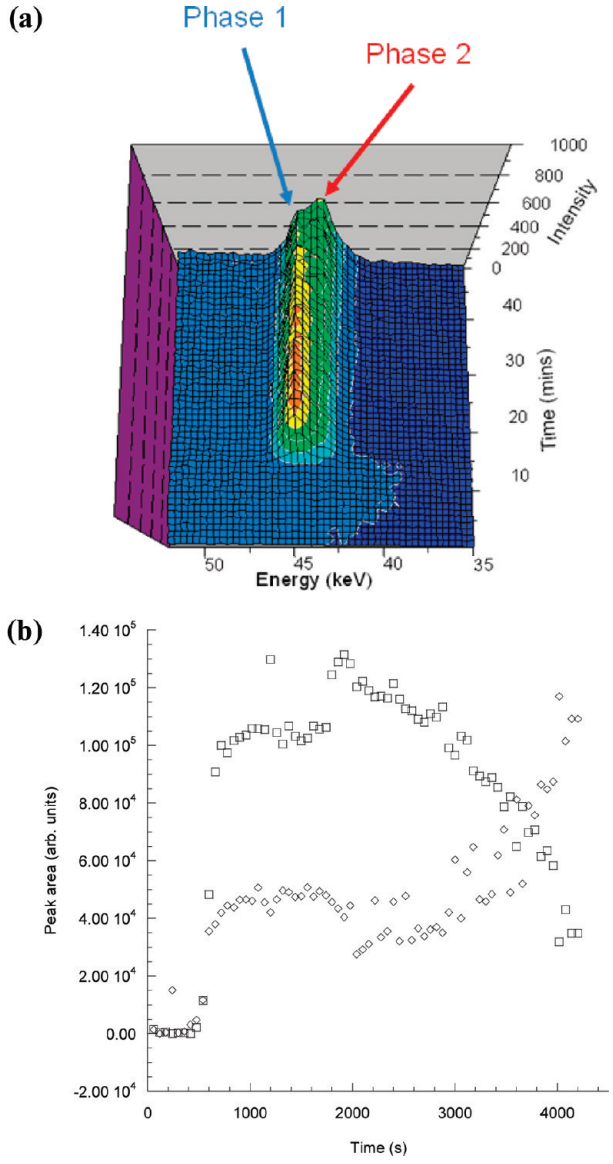

Figure 2. (a) Time-resolved in situ EDXRD spectra showing the formation of $Yb_2(OH)_5NO_3 \cdot 1.5H_2O$ at 150 °C. Two phases are apparent with *d*-spacings of 9.4 Å (42.9 keV) and 9.2 Å (44.2 keV). (b) Plot of integrated intensity for the 002 reflections of the (□) 9.2 Å (**1**) and (◇) 9.4 Å (**2**) phases, as a function of time.

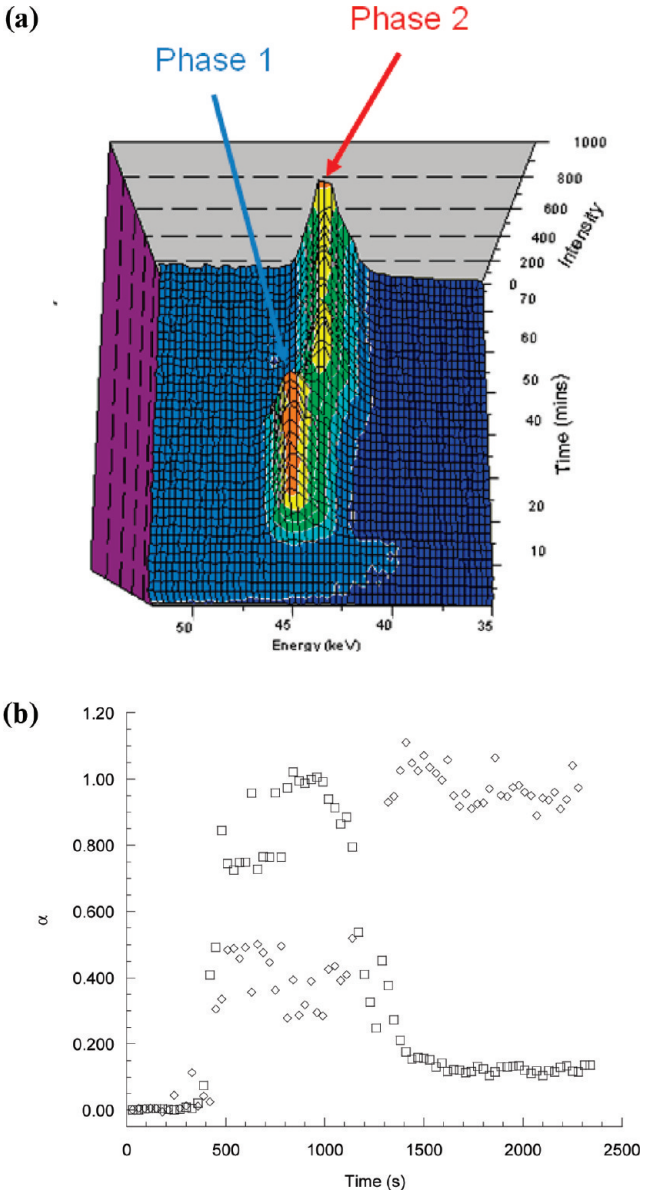

Figure 3. (a) Time resolved in situ EDXRD spectra, showing the formation of $Yb_2(OH)_5NO_3 \cdot 1.5H_2O$ at 175 °C. Two phases are apparent with *d*-spacings of 9.4 Å (42.9 keV) and 9.2 Å (44.2 keV). (b) Plot of extent of the reaction (α) for the 002 reflections of the (□) 9.2 Å (**1**) and (◇) 9.4 Å (**2**) phases, as a function of time.

~60 min, following an initial induction period of ~10 min. Analysis of the integrated intensity for each of the reflections corresponding to the interlayer separation (Figure 2b) reveals that both phases form simultaneously, with a subsequent gradual transformation of the 9.2 Å phase to the 9.4 Å phase. Repetition of these in situ experiments for the Y and Er analogues showed that only the expected 9.2 Å material is formed with no evidence for any other crystalline phases being apparent during the reactions. Data for these reactions are included in the Supporting Information.

Screening of the reaction, as a function of temperature, revealed that the product is strongly dependent on the reaction conditions. It is found that, at temperatures of 100−150 °C, the biphasic mixture is formed in ex situ experiments and this largely is reflected in the in situ experiments. Only at the lowest temperature investigated (100 °C) are differences observed, with only the 9.4 Å phase observed in situ in the first hour, although it is likely that prolonged heating at this temperature would have led to the observation of the 9.2 Å phase as well. Upon increasing the temperature to 175 °C, it was observed that the 9.2 Å phase formed first and then converted to the 9.4 Å material, as shown in Figure 3a. This reaction pathway was reproducible, making it possible to separate and isolate both the 9.2 Å and 9.4 Å phases by quenching the reaction at an appropriate point.

The 9.2 Å phase, $Yb_2(OH)_5NO_3 \cdot 1.5H_2O$ (**1**) was relatively poorly crystalline, showing few reflections other than a series of 00*l* reflections in the powder XRD pattern (Figure 4a). This phase is analogous to the recently reported $Ln_2(OH)_5NO_3 \cdot 1.5H_2O$ (Ln = Y, Gd−Tm) materials, which have been described elsewhere.[6] The characterizing

data (TGA and elemental analysis) for **1** are included in the Supporting Information and in the SEM image shown in Figure 5a, shows that the sample consists of platelike crystals that are poorly defined in shape, often with serrated edges, when compared to the morphologies observed for the previously reported $Ln_2(OH)_5NO_3 \cdot 1.5H_2O$ (Ln = Y, Gd−Tm) phases. However, note that the structures of these hydroxynitrates have not been determined and no crystals of **1** were obtained from this study.

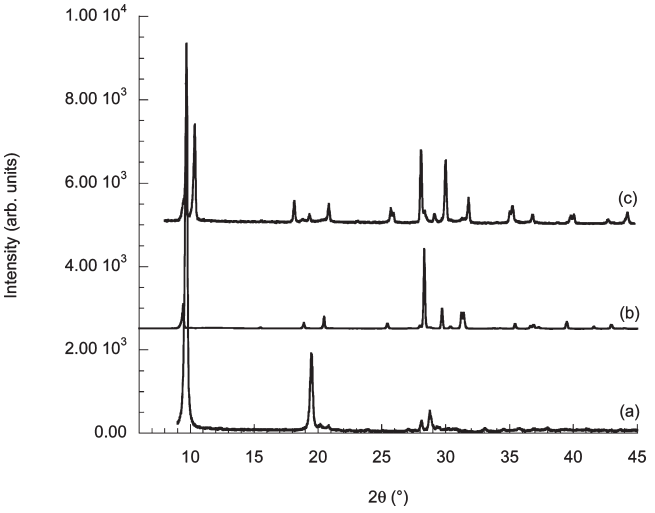

Figure 4. Powder XRD patterns of (a) **1**, (b) **2**, and (c) **3**.

In contrast, the 9.4 Å phase (**2**) was significantly more crystalline (Figure 4b), and extremely small but well-formed single crystals were present in the sample. The structure was solved from synchrotron XRD data collected from these crystals. Compound **2** crystallizes in the centrosymmetric orthorhombic space group *Cmcm* (No. 63) with the following unit-cell parameters: a = 6.0000(12) Å (sic), b = 19.589(4) Å, and c = 3.7555(8) Å. Details of the structural refinement are contained in Table 1, and the crystal structure is shown in Figure 6. The asymmetric unit contains a single Yb^{3+} ion and three O atoms, one of which is partially occupied. H atoms could not be located in this study; the distinction between bound water and hydroxide is made by reference to the structure. Each hydroxide bridges three Yb^{3+} ions, and this generates layers that are two Yb^{3+} ions thick. It seems likely, on space considerations, that the nitrate is bound to the layer. The O atom projecting into the interlayer region could correspond to the nitrate to give an overall layer $[Yb_2(OH)_5(NO_3)]$. The remainder of the nitrate is disordered and not located in this study. There is also evidence for disorder in the position of some of the hydroxide. Each Yb^{3+} ion has a formal coordination number of 8.5, indicating that the disordered hydroxide leads to variable coordination geometry; one-half of the Yb^{3+} ions are 8-coordinated, while the remainder are 9-coordinated. No interlayer species were identified from the diffraction data.

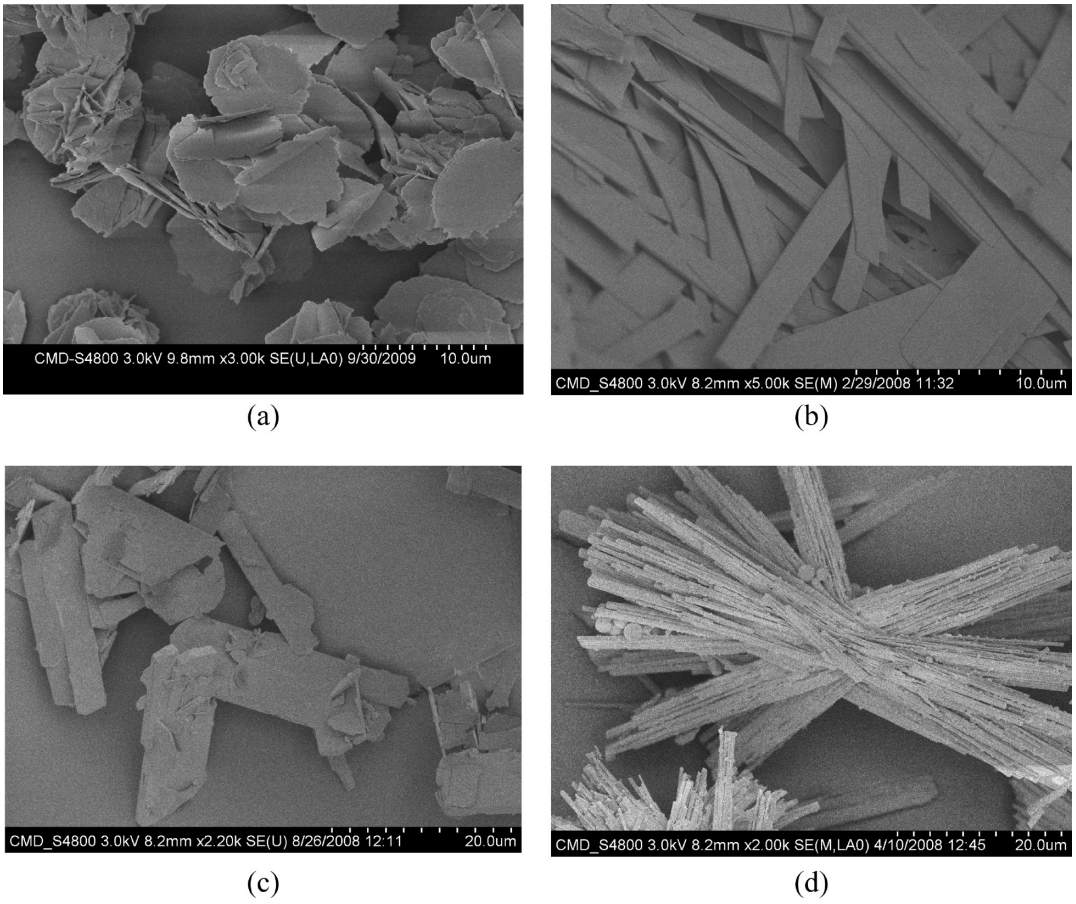

Figure 5. Scanning electron microscopy (SEM) images of (a) **1**, (b) **2**, (c) **3**, and (d) **4**.

Table 1. Crystal Data and Structural Refinement Parameters for 2 and 3

parameter	2	3
theta range for data collection	3.57°−31.78°	3.53°−30.91°
empirical formula	O7 Yb2	O3 Yb
formula weight	458.08	221.04
temperature	120(2) K	120(2) K
wavelength	0.6943 Å	0.69430 Å
crystal system	orthorhombic	orthorhombic
space group	*Cmcm*	$Pna2_1$
a	6.0000(12) Å	*a* = 33.866(5) Å
b	18.589(4) Å	*b* = 3.7305(6) Å
c	3.7555(8) Å	*c* = 5.9417(10) Å
α	90°	90°
β	90°	90°
γ	90°	90°
volume	418.87(15) $Å^3$	750.7(2) $Å^3$
Z	2	8
density (calculated)	3.632 Mg/m^3	3.912 Mg/m^3
absorption coefficient	22.168 mm^{-1}	24.722 mm^{-1}
F(000)	392	752
crystal size	0.02 mm × 0.01 mm × 0.01 mm	0.035 mm × 0.01 mm × 0.005 mm
index ranges	$-7 \le h \le 8$, $-23 \le k \le 27$, $-5 \le l \le 5$	$-49 \le h \le 48$, $-5 \le k \le 5$, $-8 \le l \le 8$
reflections collected	1582	6912
independent reflections	416 [*R*(int) = 0.0781]	1319 [*R*(int) = 0.0769]
completeness to theta = 26.00°	99.6%	99.2%
absorption correction	semiempirical from equivalents	semiempirical from equivalents
maximum and minimum transmission	0.801 and 0.668	0.7901 and 0.4380
refinement method	full-matrix least-squares on F^2	full-matrix least-squares on F^2
data/restraints/parameters	416/6/21	1319/1/35
goodness-of-fit on F^2	1.095	1.139
final *R* indices [$I > 2\sigma(I)$]	R1 = 0.0562, wR2 = 0.1395	R1 = 0.0846, wR2 = 0.2486
R indices (all data)	R1 = 0.0901, wR2 = 0.1513	R1 = 0.0959, wR2 = 0.2585
largest diffraction peak and hole	3.195 and −2.952 e/$Å^3$	11.088 and −9.101 e/$Å^3$

The unit cell contains two flat ytterbium hydroxide layers, extending in the *xz*-plane related by an inversion center. The result is layers stacked in ABAB fashion along the crystallographic *b*-axis with an interlayer separation of 9.295(4) Å. Analysis of the structure using the program PLATON[45] reveals that each unit cell contains two voids each of ~68 $Å^3$ (a total of 31.6% of the unit-cell volume). The small voids may be suitable to contain water.

The composition of the bulk sample of **2** was confirmed by a combination of elemental analysis and TGA (see Supporting Information). The TGA trace of **2** displays three distinct mass losses, comparable to those seen for other layered hydroxides. An initial mass loss of 6.67% (the calculated value for $x = 2$ is 6.81%) at <150 °C corresponds to the loss of co-intercalated water. This is followed by the partial decomposition of the layers with the loss of two water molecules. This gives rise to a mass loss of 6.91% (7.31%) by 350 °C, leaving a material of nominal composition "$Yb_2O_2(OH)NO_3$", in agreement with the proposed decomposition pathway for $Y_2(OH)_5NO_3 \cdot 1.5H_2O$.[9] Complete decomposition, to Yb_2O_3, occurs by 650 °C with a further mass loss of 12.87% (13.79%). No further mass loss is observed above 650 °C. The SEM image of **2** is shown in Figure 5b and shows that the material is microcrystalline with a rectangular plate morphology.

FTIR of **2** (Figure 7) confirms the presence of a unidentate-coordinated nitrate anion by the observation of two bands at 1339 and 1411 cm^{-1}, corresponding to the asymmetric ν_4 and symmetric ν_1 stretches of $O-NO_2$, respectively, and a third band at 1048 cm^{-1}, which is due to the ν_2 N−O stretch. This contrasts with **1**, which shows a single broadband at 1348 cm^{-1}, which is typical of an uncoordinated nitrate anion, as seen for the previously reported $Ln_2(OH)_5NO_3 \cdot 1.5H_2O$ (Ln = Y, Gd−Tm) phases. Other features include a broad absorption band at ~3500 cm^{-1}, corresponding to a combination of the stretching vibrations of the layer hydroxyl groups and the interlayer water molecules and a bending vibration of water at 1650 cm^{-1}.

At higher temperatures, the system showed even more-complex behavior with the observation of two further distinct phases. The course of the reaction at 210 °C is shown in Figure 8, from which three separate phases are apparent. As for the reaction at 175 °C, the reaction pathway was reproducible, allowing for the different phases to be isolated via quenching experiments. The first phase that forms, after an induction period of ~5 min, is the 9.4 Å phase that has been observed in the lower-temperature experiments. At this temperature, there is no evidence for the formation of the 9.2 Å phase.

After initial formation of the 9.4 Å phase, we see the appearance of a short-lived intermediate between ~34 min and ~42 min, with a *d*-spacing corresponding to 8.5 Å. Because of the fleeting nature of this phase, and despite extensive screening, it has only been observed in the in situ EDXRD experiments but has been isolated, with a small amount of the 9.4 Å phase as an impurity (see Figure 4c), by quenching. The sample was a microcrystalline powder but did contain very small single crystals of $Yb_2(OH)_5NO_3 \cdot H_2O$ (**3**). Compound **3** crystallizes in the noncentrosymmetric space group $Pna2_1$ (No. 33) with the

(45) Spek, A. L. *J. Appl. Crystallogr.* **2003**, *36*, 7.

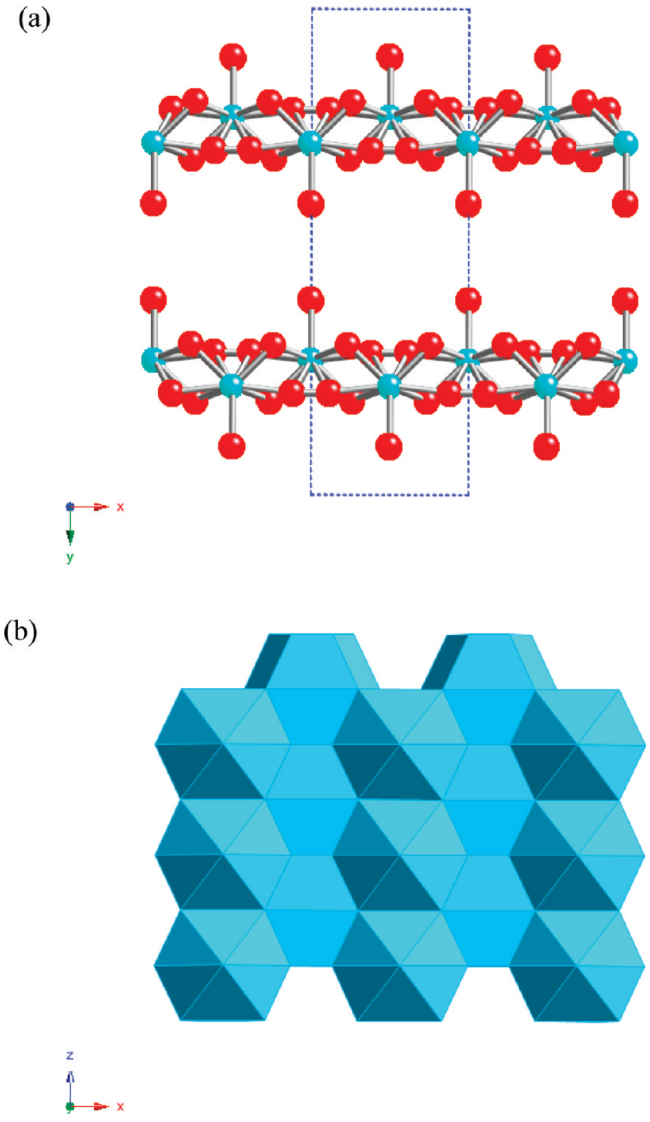

Figure 6. (a) Crystal structure and (b) polyhedral representation of a single layer of $Yb_2(OH)_5NO_3 \cdot 2H_2O$, **2**. ($Yb^{3+}$ ions are shown in blue, O atoms are shown in red).

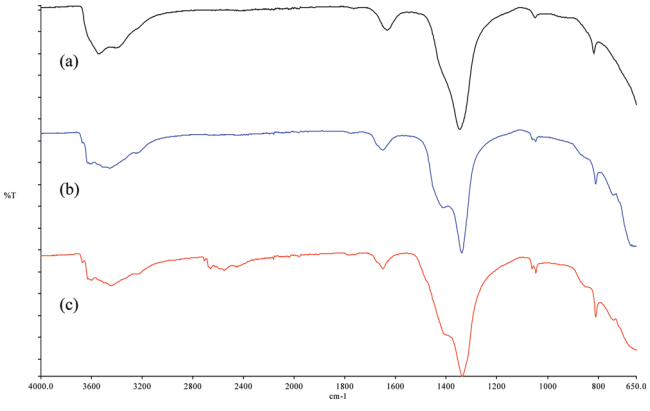

Figure 7. FTIR spectra of (a) $Yb_2(OH)_5NO_3 \cdot 1.5H_2O$ (**1**), (b) $Yb_2(OH)_5NO_3 \cdot 2H_2O$ (**2**), and (c) $Yb_2(OH)_5NO_3 \cdot H_2O$ (**3**).

following unit-cell parameters: a = 33.866(5) Å, b = 3.7305(6) Å, and c = 5.9417(10) Å. A summary of crystallographic data is contained in Table 1, and the crystal structure of **3** is shown in Figure 9. The asymmetric

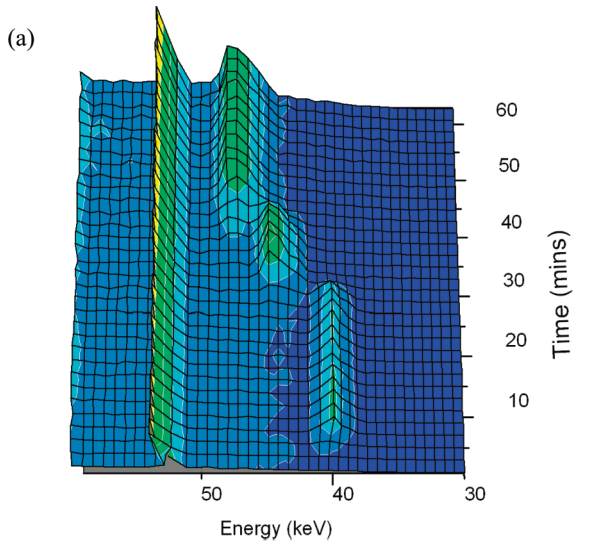

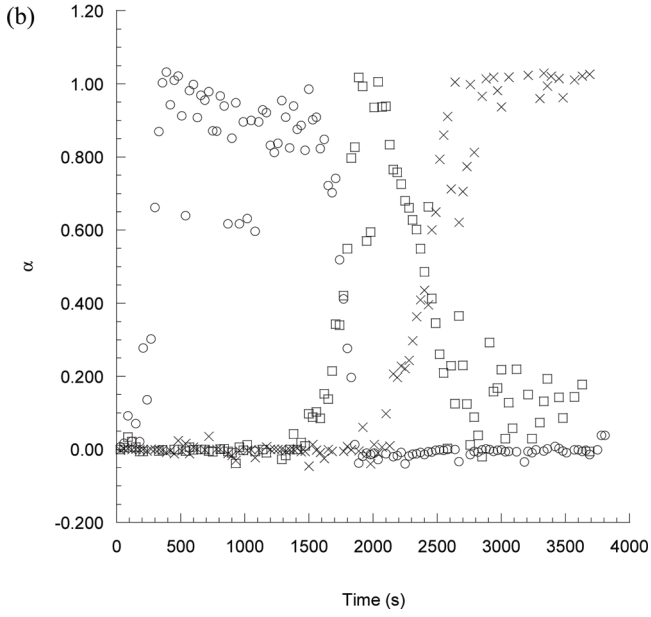

Figure 8. (a) Time-resolved in situ EDXRD spectra showing the evolution of Yb/ $OH/NO_3/H_2O$ system at 210 °C. Three phases are formed sequentially, with *d*-spacings of 9.4 Å (40.2 keV), 8.5 Å (44.6 keV), and 8.0 Å (47.2 keV). (b) Plot of extent of reaction (α) for the 002 reflections of the (○) 9.4 Å, (□) 8.5 Å, and (×) 8.0 Å phases, as a function of time. Yb Kα resonances are observed at 52.36 keV.

unit contains two independent Yb^{3+} ions, each of which is bound by three O atoms. Yb1 and O1, O2, O3 form a single layer, whereas the coordination of Yb2 by O4, O5, and O6 produces a second independent layer. O1, O2, O4, and O5 are likely to be hydroxide: each one bridges between three Yb^{3+} cations. The remaining O atoms project perpendicular to these layers, suggesting that these may be hydroxide or nitrate. H atoms were not located in this study. Assuming a 50:50 distribution of hydroxide and nitrate in these sites, the layer composition would be $Yb_2(OH)_5(NO_3)$. Additional water molecules present between the layers were not located crystallographically.

Within each layer, the Yb^{3+} cation is 7-coordinated: both Yb1 and Yb2 adopt a distorted capped trigonal prismatic geometry. In each case, the capping atom

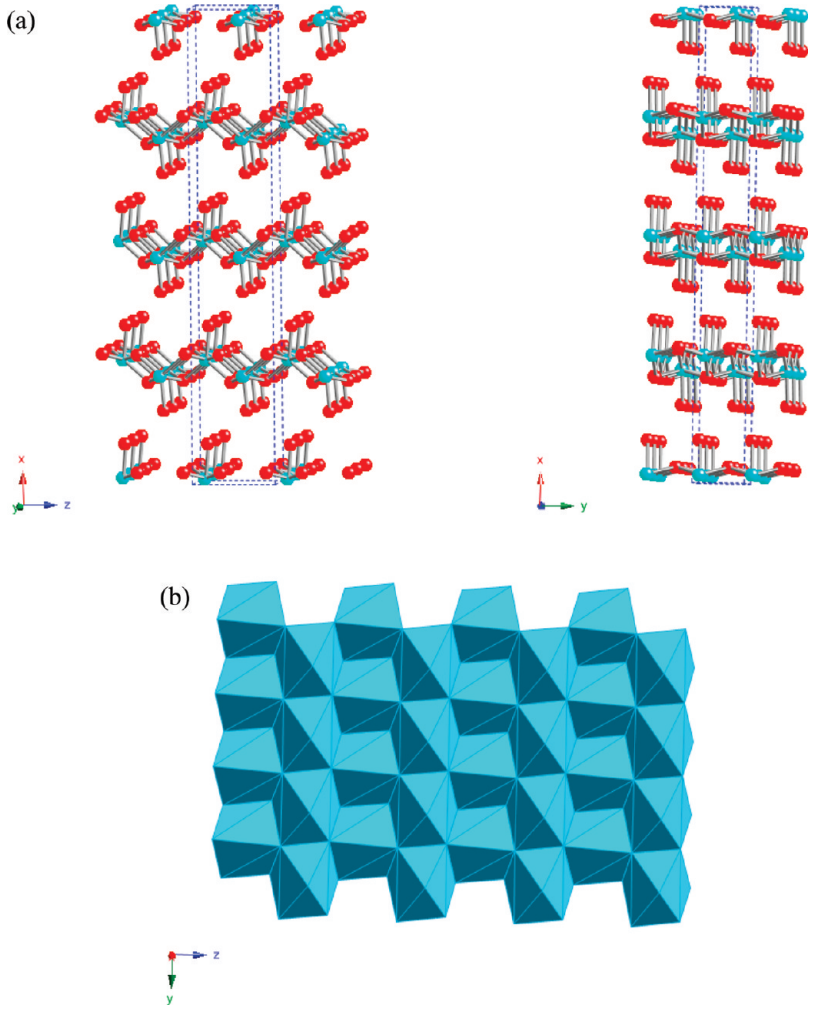

Figure 9. (a) Crystal structure and (b) polyhedral representation of a single layer of $Yb_2(OH)_5NO_3.H_2O$, **3**. (Yb^{3+} cations are represented in blue, O atoms are represented in red).

(hydroxide or nitrate) projects into the interlayer region. Each unit cell contains four layers, stacked along the crystallographic *a*-axis at a distance of 8.467(5) Å. The layers lie in an approximate AAAA orientation, although they do not directly overlie. The structure is pseudo-centrosymmetric and close to adopting the space group *Pnma*. However, introducing a center of symmetry does not allow for distortion of the Yb polyhedra. Each unit cell contains a void space of ~90 $Å^3$ within which unbound water may be located. It is likely that this phase is the same as the one that has been previously reported by Haschke as occurring as a minor impurity in the synthesis of $Ln_2(OH)_{6-x}(NO_3)_x$ materials.[7] However, that phase was not structurally characterized and reported as having a higher degree of hydration than has been found here.

The TGA data for **3** show three mass losses: an initial mass loss of 3.09% (the calculated value for the $x = 1$ phase is 3.52%) at <150 °C, corresponding to the loss of cointercalated water; a second mass loss indicates the partial decomposition of the layers, resulting in a mass loss of 8.96% (7.31%) by 350 °C, leaving a material of nominal composition "$Yb_2O_2(OH)NO_3$";[9] and a further mass loss of 12.75% (13.79%), yielding Yb_2O_3, occurs by 650 °C with no further mass loss observed at >650 °C.

FTIR spectroscopy analysis of **3** (Figure 7c) confirms the presence of a coordinated nitrate anion with two distinct bands being observed in the 1300−1500 cm^{-1} region, corresponding to the $O-NO_2$ asymmetric stretch (ν_4, 1406 cm^{-1}) and $O-NO_2$ symmetric stretch (ν_1) at 1337 cm^{-1}. This is consistent with observations on other layered hydroxynitrate phases where the nitrate anion is coordinated to the metal cation in the layer.[14] Other features of the spectrum are the ν_2 N−O stretch, seen at 1047 cm^{-1}; a broad absorption, centered at ~3500 cm^{-1} (corresponding to a combination of the stretching vibrations of the layer hydroxyl groups and the interlayer water molecules); and a bending vibration of water, at 1650 cm^{-1}. The SEM image (see Figure 5c) shows that the morphology of **3** consists of distorted rectangular plates with a much broader 001 face than that observed for 2.

The intermediate phase **3** undergoes a final transformation to $Yb_4O(OH)_9NO_3$ (**4**), which is a three-dimensional (3D) framework structure with one-dimensional (1D) channels containing uncoordinated NO_3^- ions. This a new Yb phase and is isostructural with $Y_4O(OH)_9NO_3$[46]

(46) Christensen, A. N.; Nielsen, M.; O'Reilly, K. P. J.; Wroblewski, T. *Acta Chem. Scand.* **1992**, *46*, 224.

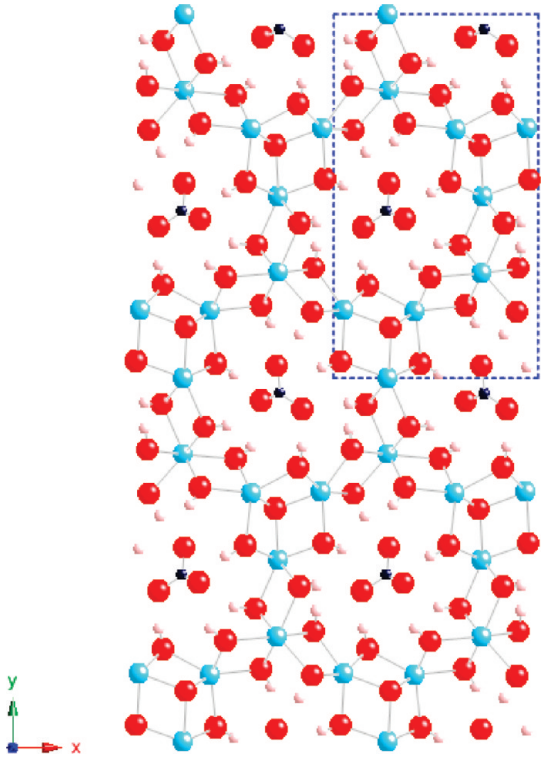

Figure 10. Crystal structure of $Yb_4O(OH)_9NO_3$. (Yb^{3+} cations are represented in blue, O atoms are represented in red, N atoms are represented in dark blue, and H atoms are represented in pink).

and $Er_4O_2(OH)_8 \cdot HNO_3$,[47] although it is likely that the proton distribution in the Er compound is incorrect. SEM imaging (Figure 5d) of this material shows that it is microcrystalline and comprised of agglomerates of needles. $Yb_4O(OH)_9NO_3$ adopts a monoclinic structure (space group $P2_1$) with unit-cell parameters of a = 9.2840(1) Å, b = 16.2425(2) Å, c = 3.5583(1) Å, β = 101.132(4)°, as determined by Rietveld refinement (R_F^2 = 0.073). The structure is shown in Figure 10, and the refinement details are included in the Supporting Information. The asymmetric unit contains four Yb^{3+} cations, three of which are 7-coordinated with a capped trigonal prismatic geometry while the fourth cation has a 9-coordinated tricapped trigonal prismatic geometry. The Yb cations are linked by μ_2 hydroxide anions forming the framework around the channels which contain the nitrate anions. The oxide ion is located in a tetrahedron of Yb^{3+} cations and is displaced toward one triangular face.

The TGA data for **4** display two distinct mass losses: (i) an initial mass loss of 7.84% at <350 °C corresponds to the decomposition of the hydroxide groups with the loss of four molecules of water (calculated mass loss = 7.81%); and (ii) complete decomposition, to Yb_2O_3, occurs by 650 °C with a further mass loss of 6.77% (6.82%). The composition of **4** was further confirmed by elemental analysis, which gave Yb = 74.55% (calculated = 74.97%), N = 1.43% (1.52%), and H = 0.91% (0.98%).

One characteristic property of layered hydroxides is their ability to undergo anion exchange reactions, and the potential of **2** and **3** in this respect has been investigated. Room-temperature anion-exchange reactions between the layered phases **2** and **3** and sodium terephthalate proved unsuccessful, providing further evidence that the nitrate anions in the layered species may be directly coordinated to the Yb^{3+} cation, as suggested by the crystal structures and characterizing data previously discussed. This would be expected to greatly reduce their capacity for anion exchange, in comparison to the $[Ln_2(OH)_5]NO_3 \cdot 1.5H_2O$ phases where the nitrate is located in the interlayer gallery and undergoes facile reactions at room temperature with a wide range of organic anions.[5,6] In the case of $La(OH)_2NO_3 \cdot H_2O$, where the nitrate is coordinated to the La^{3+} cation, it has been shown that prolonged heating at 65 °C is required to bring about complete anion exchange with acetate, benzoate, and terephthalate.[14] Under analogous conditions to these, partial exchange of terephthalate for nitrate has been achieved for both **2** and **3.** In both cases, a small amount of anion exchange was observed after 24 h with ~50% exchange being observed after 7 days. Powder XRD patterns for the reactions of **2** and **3** with terephthalate are included in the Supporting Information. However, note that the method of isolation of these phases prevented an in-depth anion exchange study from being performed. The framework structure of **4** will greatly limit its scope for anion exchange, and reactions with small inorganic anions such as chloride or carbonate proved unsuccessful. This indicates that, although the nitrate anions are uncoordinated in this phase, the channels are not readily accessible.

Kinetics and Mechanism. The time-resolved in situ EDXRD experiments also reveal a wealth of kinetic and mechanistic information about this complex system. The effect of temperature on the product formed has been described in the previous section. Sharp-Hancock analysis of the $\alpha(t)$ versus time data for the formation of **2**, as a function of temperature, is shown in Figure 11a, and the kinetic parameters obtained for all the phases are summarized in Table 2. The induction periods refer to the time taken for coherent diffraction for that phase to be observed and were used to define t = 0 for the growth of each phase. It is found that the induction period for the reaction decreases as the temperature is increased. The exponents obtained have an average value of $n \approx 2$ for phase **2**. This suggests that the two-dimensional (2D) growth of these materials is phase-boundary-controlled, following instantaneous nucleation. Confirmation that the mechanism for the formation of **2** remains constant across the temperature range investigated can be obtained from the reduced time plot shown in Figure 11b, which shows that the extent of reaction curves for each temperature are superimposable within experimental error. In addition, the rate constants can be used to obtain an estimate of the activation energy for the formation of **2**. From the plot of $\ln(k)$ vs $1/T$, shown in Figure 12, the activation energy for the hydrothermal synthesis of **2** from basic solution can be calculated to be +67 kJ/mol. This value is comparable to those determined in this way

(47) Wolcott, H. A.; Milligan, W. O.; Beall, G. W. *J. Inorg. Nucl. Chem.* **1977**, *39*, 59.

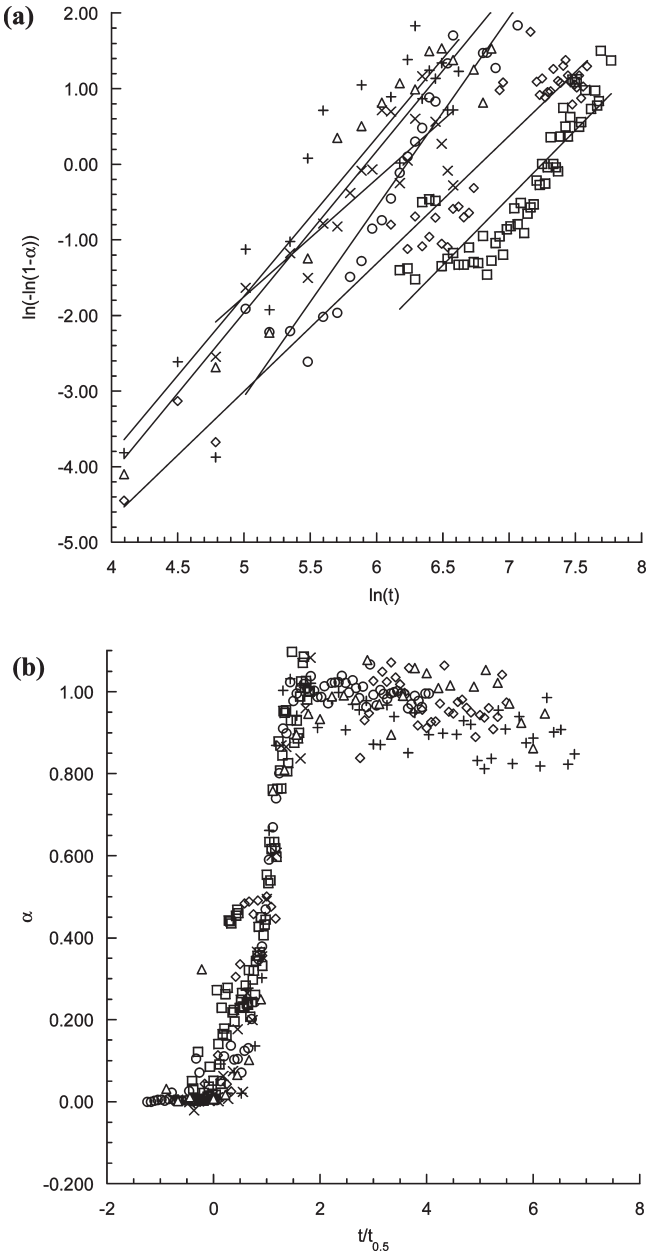

Figure 11. (a) Sharp−Hancock plots for the formation of **2** over a range of temperatures and (b) plots of extent of reaction (α) against reduced time ($t/t_{0.5}$) for the formation of **2**. (Symbol legend: (○) 100 °C, (□) 125 °C, (△) 150 °C, (◇) 175 °C, (+) 210 °C, and (×) 220 °C).

for other layered hydroxide systems including the reconstruction of Mg/Al LDHs (+41 kJ/mol) and the formation of Li/Al LDHs by the intercalation of Li salts into gibbsite (+27 kJ/mol).[48,49]

A similar kinetic analysis for the other phases reveals that the exponent for the formation of **1** has an average value of $n \approx 2.5$, suggesting a similar two-dimensional growth mechanism to that observed for **2**. The reduced time plot for **1** confirms that the mechanism remains constant across the temperature range investigated, and the activation energy for the hydrothermal synthesis of **1** can be estimated to be +29 kJ/mol. Because phases **3** and **4** are observed at fewer temperatures, a detailed analysis of the data is not possible.

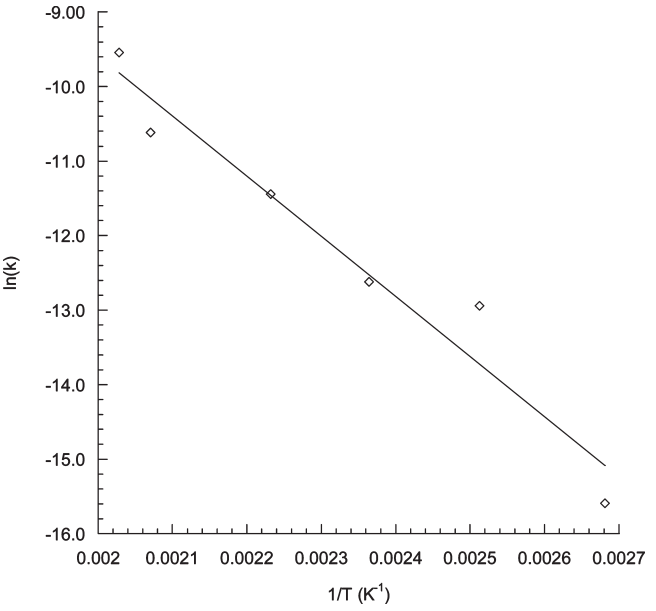

Figure 12. Arrhenius plot for the determination of the activation energy for the formation of **2**.

Table 2. Kinetic Parameters Obtained from the Sharp−Hancock Analysis of the Time Resolved In Situ EDXRD Data for 1 - 4

temperature (°C)	induction time (s)	exponent	k (s^{-1})
	1, $Yb_2(OH)_5NO_3 \cdot 1.5H_2O$, 9.2 Å Phase		
125	570	2.41	3.59×10^{-7}
150	300	2.45	2.86×10^{-7}
175	270	2.47	9.24×10^{-7}
220	150	2.60	1.55×10^{-6}
	2, $Yb_2(OH)_5NO_3 \cdot 2H_2O$, 9.4 Å Phase		
100	600	2.50	1.69×10^{-7}
125	570	1.10	2.40×10^{-6}
150	300	2.13	3.31×10^{-6}
175	300	1.69	1.07×10^{-5}
210	60	2.08	2.44×10^{-5}
220	210	1.56	7.15×10^{-5}
	3, $Yb_2(OH)_5NO_3 \cdot 1H_2O$, 8.5 Å Phase		
210	1400	2.03	4.11×10^{-6}
	4, $Yb_4O(OH)_9NO_3$		
210	1950	1.92	5.44×10^{-6}

In several of the reactions, one phase is observed to transform into another and analysis of the intersection of the $\alpha(t)$ versus time curves can provide further mechanistic information. At 175 °C, both phases **1** and **2** begin to crystallize after an induction period of ~400 s (see Figure 3b). After a short period of simultaneous growth, the crystallization of **1** becomes dominant and it is not until this phase has passed through its maximum that the growth of **2** resumes. The intersection of the two curves is located at $\alpha \approx 0.5$, which implies that the loss of coherent diffraction from **1** is matched by the gain in coherence from **2**, suggesting that the transformation is largely topotactic. In the case of the reaction at 210 °C (Figure 8b), the extent of reaction curves for both the transformation of **2** to **3** and that of **3** to **4** intersect at $\alpha \approx 0.4$, suggesting that a degree of random nucleation,

(48) Fogg, A. M.; O'Hare, D. *Chem. Mater.* **1999**, *11*, 1771.
(49) Millange, F.; Walton, R. I.; O'Hare, D. *J. Mater. Chem.* **2000**, *10*, 1713.

leading to a loss of intensity from the first phase before the growth of the second phase, is observed is apparent. Throughout this study, no evidence has been found for any of the transformations being reversible.

Conclusions

Time-resolved in situ energy-dispersive diffraction has revealed three different layered ytterbium hydroxynitrate phases with the layer composition $[Yb_2(OH)_5]^+$; $Yb_2(OH)_5NO_3 \cdot 1.5H_2O$ (interlayer separation = 9.2 Å; **1**), $Yb_2(OH)_5NO_3 \cdot 2H_2O$ (9.4 Å; **2**) and $Yb_2(OH)_5NO_3 \cdot 2H_2O$ (8.5 Å; **3**). These phases ultimately transform, at temperatures above 200 °C, to $Yb_4O(OH)_9NO_3$ (**4**), which has a 3D framework structure. Each of these phases has been isolated and the crystal structures of **2**, **3**, and **4** have been determined. Compounds **1**, **2**, and **3** differ in their degree of hydration and in the location of the nitrate anion, which is bound to the Yb^{3+} cations in **2** and **3** but is thought to be located in the interlayer gallery in **1**, based on the anion-exchange behavior. It was observed that **2** and **3** were largely resistant to anion exchange but **1** undergoes exchange readily at room temperature. The in situ diffraction investigation has also shown that **1** and **2** are formed by a two-dimensional phase-boundary-controlled growth mechanism with activation energies of +29 and +67 kJ/mol, respectively.

Acknowledgment. We thank Dr. Calum Dickinson and Mr. Gary Evans for the microscopy, EPSRC for funding (under EP/D060664/1), and STFC for access to Stations 16.4 and 9.8 of the U.K. SRS, Daresbury Laboratory. A.M.F. thanks the Royal Society for a University Research Fellowship.

Supporting Information Available: Characterizing data (XRD, TGA, IR, and elemental analysis) on the hosts and the anion-exchange derivatives reported in this paper are provided, along with the in situ diffraction data and kinetic analysis. This material is available free of charge via the Internet at http://pubs.acs.org.